

## AN EXTENSION OF THE BOUNDARY INTEGRAL METHOD APPLIED TO PERIODIC DISINFECTION OF A DYNAMIC BIOFILM\*

N. G. COGAN<sup>†</sup>

**Abstract.** Several tolerance mechanisms have been introduced to explain how bacterial biofilms are protected from disinfection. One mechanism describes the transition between two subpopulations of bacteria, one of which consumes nutrients, divides, and is susceptible to antimicrobial agents. The other subpopulation consists of dormant bacteria that are insensitive to treatments. It has been shown that the presence of this persister subpopulation can explain experimental observations of bacterial tolerance, at least in simplified domains. This investigation describes the development of a two-dimensional model of an established biofilm immersed in a flowing bulk fluid, where the biofilm influences the fluid dynamics and where the fluid flow can deform the biofilm. We introduce several extensions to this model, including the reaction between the biofilm and the antimicrobial agent, bacterial and exo-polymeric substance production, and persister dynamics. The model and numerical methods are based on the boundary integral method (BIM) but require extensions to the standard formulation to account for the production of mass within the biofilm. Our simulations indicate that many results from batch culture models carry over to the extended spatial domain. In particular, alternating dosing can eventually eliminate the bacteria but on a time scale that is much longer than in batch culture. We also predict that there is a heterogeneous distribution of persister cells that depends on the geometry of the biofilm and the dosing protocol.

**Key words.** biofilm, mathematical model, boundary integral, persister, disinfection, tolerance

**AMS subject classifications.** 35Q92, 92B08, 76T99

**DOI.** 10.1137/090745532

**1. Introduction.** Bacterial biofilms are widely understood to be sources of chronic infections, industrial corrosion, impurities, and contaminants [22, 23, 24]. Because of the negative effects of the presence of biofilms, understanding the failure of a wide range of disinfection strategies (including chemical and physical means) to eliminate biofilms is at the forefront of many investigations. It has been well established by experimental and mathematical investigations that there are a host of tolerance mechanisms that must play a role. These mechanisms include physical, physiological, and phenotypic variations. However, it is less clear how to determine which mechanism is dominant in various situations. Moreover, it is increasingly difficult to incorporate new experimental observations of the interactions between the physical structure of the biofilm with the chemical, ionic, and fluid environment.

Experimental investigations are hampered by difficulty in collecting data. In the past several years there have been many experimental advances that have yielded insight into the structure, function, and genetic expression of biofilms [43, 47, 49, 68]. However, there are several components of biofilms that are not currently available for in situ observation. For example, direct evidence of persister cells has only recently been found [36]; however, this requires destructive sampling and does not address spatial distributions.

This has led to a variety of mathematical modeling attempts, where the variables

---

\*Received by the editors January 5, 2009; accepted for publication (in revised form) March 5, 2010; published electronically April 30, 2010.

<http://www.siam.org/journals/siap/70-7/74553.html>

<sup>†</sup>Department of Mathematics, Florida State University, 208 Love Building, Tallahassee, FL 32306 (cogan@math.fsu.edu).

are transparent—possibly giving insight into the biological processes. To some degree mathematics can play a role in examining experimental hypotheses, exploring the distribution of various constituents, and predicting the outcomes of experimental designs. However, it becomes vital to precisely describe the assumptions, limitations, and testable outcomes.

In this manuscript, we describe incremental progress of a mathematical model of biofilm growth, fluid interaction, and disinfection. Although many of the components have been analyzed previously, we find that the coupling of all of the tolerance mechanisms in a spatially distributed system introduces several new predictions that can be contrasted with other models and differ from simpler uncoupled models. For this reason we argue that, although the models are becoming relatively unwieldy and unsuited to classical mathematical analysis, we are able to extend the discussion concerning biofilm disinfection.

The paper is organized as follows: section 2 introduces some biological details concerning known mechanisms, issues, and results. We also describe persister formation, which is an area where much less is known about the biological details. We also briefly review several related mathematical investigations, focusing on those that closely relate to the present research. In section 3 we describe in some detail the new components of the current model. In section 4, we describe results from several numerical simulations. Finally, we conclude with a discussion regarding the implications of our results and how these might be tested experimentally.

**2. Experimental and mathematical observations.** Although biofilms are prevalent in natural, industrial, and medical environments, one of the dominant themes is the inability to effectively clear biofilm colonies [23, 27, 32]. If standard antimicrobial or antibiotic treatments were effective, much less attention would be focused on understanding the role of the biofilm mode of existence.

Mathematics has been a partner in investigations since the term “biofilm” was coined [11]. Rather than attempt to describe the wide variety of mathematical models, we will summarize a group of modeling efforts that have focused on questions relating to disinfection. Focusing on continuum-based models will help put the current study into perspective, so we will not address the variety of cellular-automata or particle-based methods [40, 48, 67].

**2.1. Experimental observations.** Biofilms are the dominant mode of existence for most bacteria found in nature [66]. In many natural settings, biofilms can consist of a wide variety of bacteria, fungi, and protozoa. In medical and experimental settings, bacteria are the dominant active constituents and will be the only active agents that this model will include. In either case, the active components are enmeshed in a polymeric gel. The gel is primarily formed by constituents produced by the bacteria, typically collected into the term EPS (exo-polymeric substance or exo-polysaccharide). The EPS serves to anchor the bacteria in place and forms a source of protection from the environment (e.g., amoeba, macrophages, and likely antimicrobial agents and antibiotics).

Recently there has been a broader understanding concerning the relationship between the dynamics of a developing biofilm and its material properties. It is well known that the EPS endows biofilms with viscoelastic properties, allowing the biofilm to flow in response to constant stress and respond elastically to fluctuating stresses [38, 60]. In many situations it is vital to understand how the biofilm responds to various stresses, typically those from the external fluid motion. For example, large detachment events can be deadly in clinical settings. Shedding or erosion of the surface

film may not be as dangerous, since antibiotics or the secondary immune system can often eliminate individual bacteria. Moreover, it has been shown experimentally that disinfection rates depend on material properties such as viscosity [12].

In a similar direction, it has been shown that disinfection of the bacteria within a biofilm is hindered by a host of defenses. Typical defenses include physiological tolerance that stems from gradients of nutrient, and hence growth rates, within the biofilm [18, 28, 61]; physical protection that stems from degradation of the disinfectant by the EPS [58, 59]; and phenotypic resistance.

The last mechanism describes how small subpopulations of bacteria expressing a unique phenotype can evade the disinfection regime [7, 28, 46]. This resistance mechanism is different from genetic resistance, where bacteria can mutate to become a resistant strain [45]. Instead, bacteria can express a “susceptible” phenotype that multiplies if there is ample nutrient; this phenotype can be eliminated by application of an antimicrobial agent. Within any population of bacteria there is also a small fraction of “persister” cells that do not grow and are insensitive to antimicrobial agents [7, 46]. Although the mechanisms are not completely known, there is evidence of transfer between the subpopulations [35]. It is thought that this mechanism explains the biphasic survival curves, where a constant application of biocide quickly eliminates a large fraction of the population and then becomes ineffective against the remaining fraction [14, 28, 35].

**2.2. Mathematical models.** Mathematical models have also kept pace with experimental observations. It has been recognized that mathematical treatment can be used to determine various material and biological parameters [11, 17, 18, 38, 57] and that models can formalize concrete hypothesis [29]. To put the current study in perspective, we will outline a few models that show the line of development we are taking. These models are all continuum-based and are distinguished by the underlying biological concept that is explored. Roughly we will consider models that deal with the material properties of the biofilm, either with or without considering the external fluid motion, and those that deal with aspects of disinfection failure.

The first widely recognized modeling attempt was developed by Wanner and coworkers [64, 65]. This was a simple one-dimensional (in space) model that treated a slab biofilm with various nutrients. The interface between the biofilm and the fluid (e.g., the thickness) varies in response to growth and detachment. Several qualitative models of detachment and growth were considered. This model anticipates the present study in the sense that the domain was free to change in response to other dynamic variables.

A more generalized model that also treated the interface as a free boundary was developed in [29]. Here the underlying focus was on the development of a heterogeneous biofilm domain. It was shown that the heterogeneity was tied to the overall growth rate of the biofilm. A simple method of mass redistribution based on a “growth pressure” coupled mass production to interface motion. In this model the external flow was neglected, and the nutrient concentration was a dynamic variable.

By considering a slightly more detailed description of the internal composition of the biofilm, a more physical description of biomass redistribution can be addressed. Because the biofilm proper is essentially a hydro-gel with bacteria enmeshed in the long polymeric component, it is reasonable to separate the biofilm material into an elastic network and a Newtonian fluid. By assuming that, in any infinitesimal piece of biofilm, a fraction of the biofilm is network and the rest is fluid, one can develop a two-phase description of the biofilm. Each of the phases (network or fluid) is represented

by dynamic variables that introduce different stresses to the biofilm. Thus equations of motion for the biofilm follow from force balance. In the earliest version [13], the external fluid was neglected, and a growth instability similar to that in [29] could be predicted. Later the effect of the fluid motion was included in a nongrowing biofilm [18] and then in a growing biofilm [69, 70].

There have been several other models that explicitly include the external fluid motion [1, 17, 18, 31, 69, 70]. Numerical solutions of the equations governing the fluid flow and the physically heterogeneous biofilm are very difficult since the boundary separating the biofilm from the fluid is free to respond to the fluid motion and is also irregular. Standard numerical methods are computationally expensive, so alternative simplifications or treatments must be explored. One method is to treat the biofilm as an extremely viscous fluid immersed in a less viscous fluid and then translate the coupled differential equations into an integral formulation. This method, termed the boundary integral method (BIM), has been used in a variety of physical situations [50]. The advantages include reduced computational load, since the dimension of the equations is reduced, and relatively simple methods for treating heterogeneous interfaces. More details will be provided below, but typically a reciprocal relation is used to compare the unknown velocities to known velocities (singular solutions). Thus the velocities are determined based on the geometry of the interface and the relative viscosities of the “fluids.” Here we extend this treatment to include the effect of global variables including nutrient, EPS, and bacterial densities.

Concurrent with investigations into the material properties of the biofilm, there have been a host of mathematical investigations into tolerance mechanisms. Many of these treat physiological and physical mechanisms [17, 18, 30, 54, 56]. Several others focus on phenotypic tolerance or quorum-sensing impacts [3, 4, 5, 14, 16, 34, 37, 42, 62].

One example of physiological tolerance mechanisms concerns a subpopulation of the bacteria that consists of dormant and extremely tolerant bacteria, termed persister cells. Currently there is no consensus regarding the biological mechanism of persister formation. It is possible that the persister population is composed of bacteria that have undergone many division cycles; models of age-induced persistence have been introduced in a chemostat and one-dimensional setting [5, 37]. A second hypothesis assumes that the formation of persisters depends on a phenotypic response by the bacteria [7, 28, 35, 46]; it is not clear what the key to the response might be, but it is thought to be a bacterial toxin response. Several studies have analyzed various models of persister formation [7, 10, 14, 16, 42, 56]. In [16] an effort was made to generate results that distinguish the two dominant hypotheses. It was shown that, comparing models of senescence with a model of toxin regulation in a chemostat, the washout times for the persister subpopulations differed by at least one order of magnitude. This provides one testable prediction that could distinguish between the two hypotheses. One of the goals in this manuscript is to explore whether a second prediction can be obtained in a biofilm setting. In [5], numerical simulations in a one-dimensional setting indicate that the persister population dominates regions deep in the developing biofilm.

We extend our past methodology—which started with a fixed biofilm that did not respond to the fluid motion [18] and then considered the response of a nongrowing biofilm to the fluid forces and disinfection [15, 17]—to include the production of EPS and reproduction of the bacteria. This requires some attention, as the methods used previously were based directly on the BIM applied to the case of two viscous fluids with differing viscosity. This has been well studied [25, 33, 41, 50, 52, 53]. In the

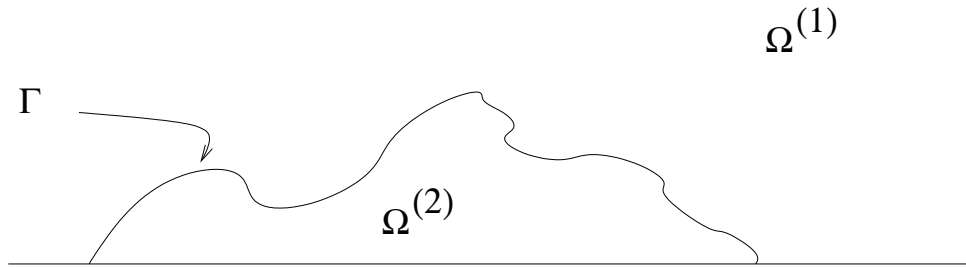


FIG. 1. Schematic of the domain. The biofilm region is denoted  $\Omega^{(2)}$ , while the fluid domain is denoted  $\Omega^{(1)}$ . The two regions are separated by the interface,  $\Gamma$ .

situation considered here, there is a source of the internal fluid. Therefore, while still incompressible, the internal fluid is not divergence-free. This alters the derivation and form of the BIM equations. Below we derive the equations for the case of an incompressible, but not divergence-free, fluid immersed in an incompressible fluid.

We also note that our previous investigations considered a homogeneous population of bacteria. Since there has been substantial interest in novel persistence mechanisms [14, 16, 18, 36, 42, 46] we have included a specialized phenotype that is tolerant to antimicrobial application. The difference here is that the phenotypes are spatially distributed and dynamic. This is important for several reasons. First, if the goal is clearing the bacterial biofilm, then understanding the location of the tolerant subpopulation could be useful. If the tolerant population is localized, this suggests that disinfection fails locally. In some situations, such as industrial settings, manual removal could be used in conjunction with disinfection protocols. A second benefit of predicting the location of the tolerant population concerns the hypothesis of persister formation. In [16] one mechanism of persister formation was included that differed from other mechanisms [5, 37]. A testable prediction was proposed to differentiate between the two mechanisms [16]. A similar prediction is made here. In [5], the persister population was located deep within the biofilm, while our results imply that the persisters are localized, but that the location is dynamic and depends on the dosing protocol.

We also find that the alternating dosing protocol proposed in chemostat and spatially homogeneous settings can be effective in a broader setting. We note that the time scale is much longer in the present setting because of the diffusion limitation. This effect is more notable if there is a reaction between the biofilm and the biocides. Predictions of the spatial distribution of persister cells typically agree with [5], where persister cells tend to be located deep within the biofilm; however, different dosing strategies and geometries can affect this.

**3. Mathematical model.** In this section we develop the components of the mathematical model which is broken down into two components: fluid/biofilm motion and the constituent kinetics. We consider the biofilm to be a viscous fluid immersed in a fluid of much less viscosity, both of which are located in a thin channel (see Figure 1). The two fluids are separated by an interface,  $\Gamma$ , that moves depending on the production of biomass by the bacteria and in response to the external fluid motion. The external fluid is assumed to be a slowly flowing Newtonian fluid that is forced through the channel by a pressure drop and whose motion is hindered by the presence of the biofilm. The nutrients and biocides are fed into the system at

the upstream entrance to the channel and are transported by diffusion and advection both in the bulk fluid and the biofilm, although we assume that the EPS introduces a diffusional barrier (e.g., the diffusion coefficient is reduced [59]). The nutrient and biocide also interact with the biofilm as detailed below. We further assume that the bacteria within the biofilm are separated into two subpopulations: persister and susceptible. There is a transfer between the two populations that is mediated by the growth-stage of the bacteria and the presence of antibiotics. Details of this model are given in section 3.2.

One of the issues when developing our model is how to approximate the solution to the developed equations. We use a mixed framework, where several of the variables are discretized onto a regular Eulerian grid (e.g., bacteria, EPS, fluid velocity) while the interface between the biofilm and the fluid is allowed to be free of the underlying grid. We use the BIM methodology to determine the motion of the interface, and a previously described method, termed regularized Stokeslets [20], to determine the fluid and biofilm velocities throughout the domain. Details are given in section 3.3.

**3.1. Two-fluid model.** We assume that the channel domain ( $0 < x < L_1$  and  $0 < y < L_2$ ) is separated into two subdomains, the bulk fluid domain  $\Omega^{(1)}$  and the biofilm domain  $\Omega^{(2)}$  (see Figure 1). Assuming typical values for fluid velocities, biofilm thickness, and viscosity, we find that the Reynolds number associated with the bulk fluid is much less than one [17]; hence the fluid momentum is governed by the Stokes equation. Since there is no mass produced, this fluid is incompressible. Thus the bulk fluid velocity  $\mathbf{U}^{(1)}$  and pressure  $P^{(1)}$  are determined by

$$(3.1) \quad \nabla \cdot \sigma^{(1)} = 0,$$

$$(3.2) \quad \nabla \cdot \mathbf{U}^{(1)} = 0,$$

where the fluid stress is given by the fluid pressure and the viscous stress:  $\sigma^{(1)} = P^{(1)}\mathbf{I} + \mu^{(1)}(\nabla\mathbf{U}^{(1)} + \nabla\mathbf{U}^{(1)T})$ . Equations (3.1) and (3.2) govern the dynamics within  $\Omega^{(1)}$ .

Although the biofilm is a viscoelastic fluid, we use a separation of time scales between the relaxation scale (on the order of seconds) and disinfection (on the order of hours) and treat the biofilm as an extremely viscous fluid, as in [17]. Since both EPS and bacteria are produced, the biofilm is not divergence-free (although it is still incompressible [8, 17]). Therefore the governing equations in  $\Omega^{(2)}$  are

$$(3.3) \quad \nabla \cdot \sigma^{(2)} = 0,$$

$$(3.4) \quad \nabla \cdot \mathbf{U}^{(2)} = R(S, A, B, E).$$

Here the fluid stress is given by the fluid pressure, the viscous stress, and an extra pressure that ensures that the biofilm is incompressible:

$$\sigma^{(2)} = \left( P^{(2)}\mathbf{I} - \frac{2}{3}\mu^{(2)}R(S, A, B, E) \right) \mathbf{I} + \mu^{(2)} \left( \nabla\mathbf{U}^{(2)} + \nabla\mathbf{U}^{(2)T} \right),$$

where the biofilm stress is  $\sigma^{(2)}$ ,  $\mathbf{U}^{(2)}$  denotes the biofilm velocity, and  $\mu^{(2)}$  denotes the biofilm viscosity.

The term  $R(S, A, B, E)$  represents a rate of mass production from both bacterial division and EPS production. Thus  $R$  depends on the nutrient, antimicrobial, bacteria, and EPS, denoted  $S$ ,  $A$ ,  $B$ , and  $E$ , respectively. We will assume throughout this investigation that the rate of mass produced is the sum of polymer and

bacterial rates,  $R = R_{eps} + R_{bacteria}$ . Bacterial growth is well described by Michaelis–Menton kinetics,  $R_{bacteria} = \frac{\mu_s S}{K_S + S} B$ , where  $\mu_s$  and  $K_S$  denote the maximum specific growth rate and half-saturation, respectively. Following [39], we assume that EPS production includes a substrate-sufficient (e.g., growth rate-limited) and a starvation condition. Thus  $R_{eps} = (k_1 \frac{K_S}{K_S + S} + k_2 \frac{S}{K_S + S}) B$ , where  $k_1$  and  $k_2$  are maximal production rates that include the rate of conversion of nutrient into EPS. This is similar to the Leudeking/Piret approach discussed in [55]. We also note that the qualitative behavior observed in our simulations does not depend heavily on the form of the EPS production component.

The velocities and pressures within the subregions must satisfy a continuity condition and a jump condition [44, 50]. The BIM framework deals with these constraints transparently, so we will wait to describe the mathematical conditions for a moment.

A typical BIM method translates the governing PDEs into an integral equation whose domain is the interface between the two domains by using a reciprocal relation. This has been done in many different places for two incompressible fluids [25, 33, 50, 52, 53]. Because one of our materials (the biofilm) is not divergence-free we obtain a different reciprocal relation.

One related version of this has been explored in [51], but there the internal fluid was a compressible gas, which substantially changes the methodology since the volume change is coupled through the pressure. Another description, closer in methodology to the method developed here, has been described in [26], where the Lorenz reciprocal relation for a compressible foam is developed. The primary difference here is that the mass production is not constant and cannot be simplified in the manner proposed in [26]. To develop the appropriate equations an approximation method requires additional consideration of the classical derivation. This leads to an integral equation that, unfortunately, contains a nonlocal term. It would seem that this limits the benefits of using BIM. However, we are able to relate the additional term to the growth function. This, along with the linearity of the equations, allows for a simple method for including this term, extending the utility of the standard method.

Below we introduce the derivation of the BIM equations. The notation we use requires specifying the particular part of the domain or the relevant equation. We denote the variables evaluated in the bulk region with a superscript,  $(*)^{(1)}$ , while those in the biofilm region are denoted  $(*)^{(2)}$ . The particular fundamental solution that we consider is the free space Greens’ function and is denoted  $(*)'$ . For variables that are vector-valued we use boldface, although at times we refer to the components of the vector, noted by the subscript  $j$ . We begin with the fundamental solution of the incompressible Stokes equations (also termed the Stokeslet solution):

$$(3.5) \quad \nabla \cdot \sigma' = \mathbf{f} \delta(\mathbf{x} - \mathbf{x}_0),$$

$$(3.6) \quad \nabla \cdot \mathbf{U}' = 0,$$

where  $\sigma' = -P' \mathbf{I} + \mu(\nabla \mathbf{U}' + \nabla \mathbf{U}'^T)$ . This is a convenient flow to use since the solution can be computed easily using Fourier transforms [50]. In two spatial dimensions the solution is

$$(3.7) \quad \begin{aligned} \mathbf{U}'(\mathbf{x}) &= -\frac{\mathbf{f}}{4\pi\mu} \ln(r) + (\mathbf{f} \cdot \mathbf{x}) \frac{\mathbf{x}}{4\pi\mu r^2} \\ &= -\frac{\mathbf{f}}{4\pi\mu} \mathbf{G}, \end{aligned}$$

where  $r = \|\mathbf{x} - \mathbf{x}_0\|$  and  $\mathbf{G}$  is the two-dimensional Stokeslet.

The free space Green's function and related stress tensor can be obtained using a variety of methods [20, 21, 50], but in two dimensions they are given by

$$(3.8) \quad \mathbf{G}_{ij}(\mathbf{x}) = -\delta_{ij} \ln r + \frac{(\mathbf{x} - \mathbf{x}_0)_i (\mathbf{x} - \mathbf{x}_0)_j}{r^2},$$

$$(3.9) \quad \mathbf{T}_{ijk} = -4 \frac{(\mathbf{x} - \mathbf{x}_0)_i (\mathbf{x} - \mathbf{x}_0)_j (\mathbf{x} - \mathbf{x}_0)_k}{r^4},$$

where  $r = |\mathbf{x} - \mathbf{x}_0|$ .

The corresponding pressure is

$$(3.10) \quad P' = \frac{(\mathbf{f} \cdot \mathbf{x})}{2\pi r^2}.$$

We use  $\mathbf{U}'$  and  $P'$  to obtain information about the biofilm flow  $\mathbf{U}^{(2)}$  and  $P^{(2)}$  starting with the component form of  $\nabla \cdot (\mathbf{U}^{(2)} \sigma') - \nabla \cdot (\mathbf{U}' \sigma^{(2)})$  and understanding summation over repeated indexes:

$$(3.11) \quad \begin{aligned} \frac{\partial}{\partial x_j} (\mathbf{U}_i^{(2)} \sigma'_{ij} - \mathbf{U}'_i \sigma_{ij}^{(2)}) &= \frac{\partial \mathbf{U}_i^{(2)}}{\partial x_j} \sigma'_{ij} - \frac{\partial \mathbf{U}'_i}{\partial x_j} \sigma_{ij}^{(2)} \\ &+ \mathbf{U}_i^{(2)} \frac{\partial \sigma'_{ij}}{\partial x_j} - \mathbf{U}'_i \frac{\partial \sigma_{ij}^{(2)}}{\partial x_j}. \end{aligned}$$

Considering the first two terms on the right-hand side, we obtain

$$\begin{aligned} &\frac{\partial \mathbf{U}_i^{(2)}}{\partial x_j} \sigma'_{ij} - \frac{\partial \mathbf{U}'_i}{\partial x_j} \sigma_{ij}^{(2)} \\ &= \frac{\partial \mathbf{U}_i^{(2)}}{\partial x_j} \left( -P' \delta_{ij} + \mu \left( \frac{\partial \mathbf{U}'_i}{\partial x_j} + \frac{\partial \mathbf{U}'_j}{\partial x_i} \right) \right) \\ &\quad - \frac{\partial \mathbf{U}'_i}{\partial x_j} \left( P^{(2)} - \frac{2}{3} \mu R \delta_{ij} + \mu \left( \frac{\partial \mathbf{U}_i^{(2)}}{\partial x_j} + \frac{\partial \mathbf{U}_j^{(2)}}{\partial x_i} \right) \right) \\ &= P' \frac{\partial \mathbf{U}_i^{(2)}}{\partial x_i} + \left( P^{(2)} + \frac{2}{3} \mu R \right) \frac{\partial \mathbf{U}'_i}{\partial x_i} \\ &\quad + \mu \left( \frac{\partial \mathbf{U}_i^{(2)}}{\partial x_j} \frac{\partial \mathbf{U}'_i}{\partial x_j} - \frac{\partial \mathbf{U}'_i}{\partial x_j} \frac{\partial \mathbf{U}_i^{(2)}}{\partial x_j} + \frac{\partial \mathbf{U}_i^{(2)}}{\partial x_j} \frac{\partial \mathbf{U}_j^{(2)}}{\partial x_i} - \frac{\partial \mathbf{U}'_i}{\partial x_j} \frac{\partial \mathbf{U}_j^{(2)}}{\partial x_i} \right). \end{aligned}$$

The first term in the last step is exactly  $-P'R$ , while the second term is zero since  $\mathbf{U}'$  is incompressible. The last terms cancel when the indices are exchanged. Therefore

$$\begin{aligned} \frac{\partial \mathbf{U}_i^{(2)}}{\partial x_j} \sigma'_{ij} - \frac{\partial \mathbf{U}'_i}{\partial x_j} \sigma_{ij}^{(2)} &= -P'R \\ &= R \nabla \left( \frac{1}{r} \right) \end{aligned}$$

since  $P' = \nabla \left( \frac{1}{r} \right)$ .

We now consider the last two terms of (3.11),

$$\begin{aligned} & \mathbf{U}^{(2)}_i \frac{\partial \sigma'_{ij}}{\partial x_j} - \mathbf{U}'_i \frac{\partial \sigma^{(2)}_{ij}}{\partial x_j} \\ &= \mathbf{U}^{(2)}_i \left[ -\frac{\partial P'}{\partial x_j} \delta_{ij} + \mu \left( \frac{\partial^2 \mathbf{U}'_i}{\partial x_j^2} + \frac{\partial^2 \mathbf{U}'_i}{\partial x_j \partial x_i} \right) \right] \\ & \quad - \mathbf{U}'_i \left[ \frac{\partial}{\partial x_j} \left( P^{(2)} - \frac{2}{3} \mu^{(2)} R(S, \mathbf{x}) \right) \delta_{ij} + \mu^{(2)} \left( \frac{\partial^2 \mathbf{U}^{(2)}_i}{\partial x_j^2} + \frac{\partial^2 \mathbf{U}^{(2)}_i}{\partial x_j \partial x_i} \right) \right], \end{aligned}$$

where each term in brackets on the right-hand side is replaced with the right-hand side of the corresponding PDE.

Putting everything together, we obtain the generalized reciprocal relation for the fluid/biofilm dynamics,

$$(3.12) \quad \nabla \cdot (\mathbf{U}\sigma') - \nabla \cdot (\mathbf{U}'\sigma) = \mathbf{f}\delta(\mathbf{x} - \mathbf{x}_0)\mathbf{U} + R\nabla \left( \frac{1}{r} \right).$$

We are now ready to transform the equations of motion for the biofilm and the ambient fluid from the reciprocal relations. We consider first the flow due to the application of a point force at a point in the bulk fluid region,  $\Omega^{(1)}$ . The boundary integral representation of the  $j$ th component of the flow is

$$(3.13) \quad \begin{aligned} U_j^{(1)}(\mathbf{x}_0) &= -\frac{1}{4\pi\mu^{(1)}} \int_{\Gamma} \sigma_{ik}^{(1)} \eta_k(\mathbf{x}) \mathbf{G}_{ij}(\mathbf{x}, \mathbf{x}_0) dl(\mathbf{x}) \\ & \quad + \frac{1}{4\pi} \int_{\Gamma} U_i(\mathbf{x}) \mathbf{T}_{ijk}(\mathbf{x}, \mathbf{x}_0) \eta_k(\mathbf{x}) dl(\mathbf{x}). \end{aligned}$$

Considering the internal flow due to a force at the same point, we obtain

$$(3.14) \quad \begin{aligned} 0 &= \int_{\Gamma} \sigma_{ik}^{(2)} \eta_k(\mathbf{x}) \mathbf{G}_{ij}(\mathbf{x}, \mathbf{x}_0) dl(\mathbf{x}) - \mu^{(2)} \int_{\Gamma} U_i(\mathbf{x}) \mathbf{T}_{ijk}(\mathbf{x}, \mathbf{x}_0) \eta_k(\mathbf{x}) dl(\mathbf{x}) \\ & \quad - \int_{\Omega} R\nabla \frac{1}{r} dV. \end{aligned}$$

Combining these two equations yields an integral equation involving the jump in the surface force  $\Delta\sigma = (\sigma^{(1)} - \sigma^{(2)})$ ,

$$(3.15) \quad \begin{aligned} U_j^{(1)}(\mathbf{x}_0) &= -\frac{1}{4\pi\mu^{(1)}} \int_{\Gamma} \Delta\sigma_{ik} \eta_k \mathbf{G}_{ij}(\mathbf{x}, \mathbf{x}_0) dl(\mathbf{x}) \\ & \quad + \frac{1-\lambda}{4\pi} \int_{\Gamma} U_i(\mathbf{x}) \mathbf{T}_{ijk}(\mathbf{x}, \mathbf{x}_0) \eta_k(\mathbf{x}) dl(\mathbf{x}) \\ & \quad - \frac{1}{4\pi\mu^{(1)}} \int_{\Omega} R\nabla \frac{1}{r} dV, \end{aligned}$$

where  $\lambda = \frac{\mu^{(2)}}{\mu^{(1)}}$ . We note that the last term in this equation comes from mass produced in the biofilm and is a volume integral which cannot be moved onto the interface.

We now perform similar computations in  $\Omega^{(2)}$ , yielding

$$(3.16) \quad \begin{aligned} U_j^{(2)}(\mathbf{x}_0) &= -\frac{1}{4\pi\mu^{(2)}} \int_{\Gamma} \Delta\sigma_{ik} \eta_k \mathbf{G}_{ij}(\mathbf{x}, \mathbf{x}_0) dl(\mathbf{x}) \\ & \quad + \frac{1-\frac{1}{\lambda}}{4\pi} \int_{\Gamma} U_i(\mathbf{x}) \mathbf{T}_{ijk}(\mathbf{x}, \mathbf{x}_0) \eta_k(\mathbf{x}) dl(\mathbf{x}) \\ & \quad - \frac{1}{4\pi\mu^{(2)}} \int_{\Omega} R\nabla \left( \frac{1}{r} \right) dV. \end{aligned}$$

Again, the last term in this equation comes from mass produced in the biofilm. A velocity field for the entire domain,  $\mathbf{U}$ , is given by joining the velocity in  $\Omega^{(1)}$  and  $\Omega^{(2)}$ . This velocity field is continuous and is valid throughout the domain.

**3.2. Constituent transport.** Once we know the velocity field throughout the domain, we are in a position to describe the dynamics of the various constituents. We are concerned with the distribution of nutrient ( $S$ ), antimicrobial ( $A$ ), bacteria ( $B$ ), and EPS ( $E$ ).

*Nutrient and antimicrobial.* Nutrient concentration changes due to advection, diffusion, and consumption by the bacteria. The diffusion of chemical constituents is fast compared to the time scale of biofilm motion, so we describe the concentrations of nutrient,  $S(\mathbf{x}, t)$ , and antimicrobial agent,  $A(\mathbf{x}, t)$ , by reaction-diffusion-advection equations at quasi-steady state,

$$(3.17) \quad \mathbf{U}(\mathbf{x}, t) \cdot \nabla S(\mathbf{x}, t) = \nabla \cdot (D_s \nabla S(\mathbf{x}, t)) - \mu_s \frac{S}{K_S + S} B(\mathbf{x}, t),$$

$$(3.18) \quad \mathbf{U}(\mathbf{x}, t) \cdot \nabla A(\mathbf{x}, t) = \nabla \cdot (D_a \nabla A(\mathbf{x}, t)) - F(A, E),$$

where  $B$  denotes the bacterial concentration. The solid components of the biofilm hinder the diffusion, so the diffusion coefficients  $D_s(\mathbf{x})$  and  $D_a(\mathbf{x})$  are smaller in the biofilm region than in the bulk flow region, with reduction factors denoted by  $r_s$  and  $r_a$ , respectively. This complicates the numerical solution of the equations since care must be taken to obtain accurate approximations near the interface. This has been described earlier [18].

The consumption of nutrient by the bacteria is modeled by Monod kinetics, where  $\mu_s$  and  $K_S$  denote the maximum specific consumption rate and Monod coefficient, respectively. The maximum consumption rate is related to the maximum growth rate through the yield rate. In particular the ratio of the consumption rate to the growth rate indicates the amount of substrate required to produce a unit mass of biomass. Both nutrient and antimicrobial enter the system at the upstream end of the channel, so Dirichlet boundary conditions are applied at  $x = 0$ . Standard outflow conditions are applied at the effluent end of the channel. At the walls of the channel we apply no-flux boundary conditions.

The reaction term,  $F$ , in (3.18) depends on the antimicrobial agent, since some agents are highly reactive with components of the biofilm (e.g., chlorine). For others, such as ciprofloxacin and chlorosulfamate, the reduction has been shown to be negligible [2]. In previous studies, we have assumed that there is no reaction [17]; however, understanding the distribution and dynamics of persister formation will require us to address possible penetration limitation. For simplicity we will assume that there may be a stoichiometric reaction between the polymer and the antimicrobial that degrades both players [10, 18]. We assume that  $F = \kappa Y_n A E$ , where  $\kappa$  denotes the reaction rate,  $Y_n$  the reaction yield (e.g., the amount of antibiotic consumed relative to EPS consumed), and  $E$  the EPS concentration (described below). This is the simplest possibility among several other forms that might be chosen [59]. Whether  $F$  is present or not will be specified in the simulations.

*Bacteria.* Following several ODE studies [14, 16, 42], we will split the bacteria into two subpopulations: susceptible ( $B_s$ ) and persister ( $B_p$ ). Each of these components are advected by the biofilm motion and transition between subpopulations depending on the local nutrient concentration. The susceptible bacteria consume nutrients and are killed by the antimicrobial. The disinfection model that we use assumes that the disinfection rate is proportional to the product of the growth rate and the antimi-

crobial concentration, with proportionality constant  $k_d$  [14, 18]. The transition rate from susceptible to persister is assumed to be proportional to the growth rate, with proportionality constant  $k_l$ . If there is no antimicrobial present, persisters can revert to susceptibles at a rate  $k_g$ . Collecting these terms, we obtain

$$(3.19) \quad \frac{\partial B_s}{\partial t} + \nabla \cdot (\mathbf{U}B_s) = \left[ (1 - k_d(A) - k_l) \frac{S}{K_s + S} B(\mathbf{x}, t) \right] + k_g B_p,$$

$$(3.20) \quad \frac{\partial B_p}{\partial t} + \nabla \cdot (\mathbf{U}B_p) = k_l \frac{S}{K_s + S} B_s - k_g B_p,$$

where  $B_s$  and  $B_p$  are zero outside the biofilm region. The coefficient  $k_d$  reflects the particular biocide. In this investigation we are not comparing the results for differing biocides, so  $k_d$  is constant. Other forms of the disinfection rate have been investigated where more sophisticated disinfection models are developed [14, 18, 54, 56]. A full discussion of the relevance of the kinetics on the right-hand sides is given in [14]. We apply no-flux conditions at the channel walls and Dirichlet conditions ( $B = 0$ ) at the influent end. At the effluent end we impose outflow conditions allowing the bacteria to be transported out of the domain; however, we have ensured that our computational domain is sufficiently large that the cluster does not reach the end of the domain.

*EPS.* The final component that we need to describe is the EPS; since the motion of the biofilm domain depends on the production of mass and EPS may affect the antimicrobial, we include this as a state variable. Although sophisticated models have been introduced to handle this component [6, 39], we will assume a very simple reaction-advection equation, where the change in EPS, which is denoted  $E$ , is balanced by production by the bacteria (as described above) and degradation by the antimicrobial:

$$(3.21) \quad \frac{\partial E}{\partial t} + \nabla \cdot (\mathbf{U}E) = \left( k_1 \frac{K_S}{K_S + S} + k_2 \frac{S}{K_S + S} \right) B - \frac{R}{Y_n}.$$

We are assuming that the persister subpopulation does not contribute to the production of polymer since they appear to be dormant [28, 46].

*Final equations.* The final system of equations and boundary conditions that we have are collected here for completeness. The first set describes the velocity of the bulk fluid and biofilm region:

$$(3.22) \quad \begin{aligned} U_j^{(1)}(\mathbf{x}_0) &= -\frac{1}{4\pi\mu^{(1)}} \int_{\Gamma} \Delta\sigma_{ik}\eta_k \mathbf{G}_{ij}(\mathbf{x}, \mathbf{x}_0) dl(\mathbf{x}) \\ &\quad + \frac{1-\lambda}{4\pi} \int_{\Gamma} U_i(\mathbf{x}) \mathbf{T}_{ijk}(\mathbf{x}, \mathbf{x}_0) \eta_k(\mathbf{x}) dl(\mathbf{x}) \\ &\quad - \frac{1}{4\pi\mu^{(1)}} \int_{\Omega} R \nabla \frac{1}{r} dV, \end{aligned}$$

$$(3.23) \quad \begin{aligned} U_j^{(2)}(\mathbf{x}_0) &= -\frac{1}{4\pi\mu^{(2)}} \int_{\Gamma} \Delta\sigma_{ik}\eta_k \mathbf{G}_{ij}(\mathbf{x}, \mathbf{x}_0) dl(\mathbf{x}) \\ &\quad + \frac{1-\frac{1}{\lambda}}{4\pi} \int_{\Gamma} U_i(\mathbf{x}) \mathbf{T}_{ijk}(\mathbf{x}, \mathbf{x}_0) \eta_k(\mathbf{x}) dl(\mathbf{x}) \\ &\quad - \frac{1}{4\pi\mu^{(2)}} \int_{\Omega} R \nabla \left( \frac{1}{r} \right) dV. \end{aligned}$$

We note that the method that we use to determine the velocity does not require solving these equations for every point in the domain. Instead we use this to determine

the velocity of a finite number of marker points on the interface. We then use the method of regularized Stokeslets to determine the velocity away from the boundary. This is described in detail in the next section. This method also allows us to impose no-slip boundary conditions at  $y = 0$  and  $y = L_2$  by including the solid boundaries as locations where the velocity is zero. This is a relatively standard technique used in the method of regularized Stokeslets [17, 20]. Moreover, we do not need to impose inflow or outflow conditions, as these arise naturally from the interaction between the parabolic background flow and the forces that are applied to enforce the no-slip and boundary motion in the numerical method.

The diffusible substances (e.g., nutrient and antimicrobial) are governed by

$$(3.24) \quad \mathbf{U}(\mathbf{x}, t) \cdot \nabla S(\mathbf{x}, t) = \nabla \cdot (D_s \nabla S(\mathbf{x}, t)) - \mu_s \frac{S}{K_S + S} B(\mathbf{x}, t),$$

$$(3.25) \quad \mathbf{U}(\mathbf{x}, t) \cdot \nabla A(\mathbf{x}, t) = \nabla \cdot (D_a \nabla A(\mathbf{x}, t)) - F(A, P).$$

The boundary conditions are

$$\begin{aligned} \frac{\partial S}{\partial \eta} \Big|_{y=0, L_2} &= 0, \\ \frac{\partial A}{\partial \eta} \Big|_{y=0, L_2} &= 0, \\ S|_{x=0} &= C_S(t), \\ A|_{x=0} &= C_A(t), \end{aligned}$$

with standard outflow conditions at  $y = L_2$ , which means that the nutrient is allowed to exit the system by fluid advection.

The components of the biofilm are governed by

$$(3.26) \quad \frac{\partial B_s}{\partial t} + \nabla \cdot (\mathbf{U}B_s) = \left[ (1 - k_d(A) - k_l) \frac{S}{K_S + S} B(\mathbf{x}, t) \right] + k_g B_p,$$

$$(3.27) \quad \frac{\partial B_p}{\partial t} + \nabla \cdot (\mathbf{U}B_p) = k_l \frac{S}{K_S + S} B_s - k_g B_p,$$

$$(3.28) \quad \frac{\partial E}{\partial t} + \nabla \cdot (\mathbf{U}E) = \left( k_1 \frac{K_S}{K_S + S} + k_2 \frac{S}{K_S + S} \right) B - R/Y_n.$$

The boundary conditions are

$$\begin{aligned} \frac{\partial B_s}{\partial \eta} \Big|_{y=0, L_2} &= 0, & \frac{\partial B_s}{\partial \eta} \Big|_{x=L_1} &= 0, & B_p|_{x=0} &= 0, \\ \frac{\partial B_p}{\partial \eta} \Big|_{y=0, L_2} &= 0, & \frac{\partial B_p}{\partial \eta} \Big|_{x=L_1} &= 0, & B_p|_{x=0} &= 0, \\ \frac{\partial E}{\partial \eta} \Big|_{y=0, L_2} &= 0, & \frac{\partial E}{\partial \eta} \Big|_{x=L_1} &= 0, & E|_{x=0} &= 0. \end{aligned}$$

As mentioned above, we do not use (3.15) and (3.16) to determine the velocity throughout the domain. Instead we apply methods developed in [17, 20] to simplify this step. This is discussed in the next section, as are the numerical methods used for the rest of the equations.

**3.3. Numerical methods.** We first focus on the components of the fluid equations ((3.22) and (3.23)) that enter because of growth. In early models, we described the three-part method that includes discretizing the interface, solving the integral equation at each of the discrete points, and using these velocities and the method of regularized Stokeslets [20] to determine the velocity at each point in the discretized domain [15, 17]. Our approach here is similar, but we must address the volume integral as well as the altered stress. We take a straightforward approach to including the volume integral: since the pressure caused by a source is known analytically through the Stokeslet, for each point in the domain, we use a trapezoidal approximation to the volume integral. This is computationally expensive but needs only to be calculated for  $N$  different interface points.

To include the altered surface traction terms,  $\Delta\sigma = (\sigma^{(1)} - \sigma^{(2)})$ , we exploit the linearity of the integral equations. We split the surface traction into two parts. The first is the “standard” traction:  $\Delta\sigma^{standard} = \sigma^1 - \sigma^2 = -P^1\mathbf{I} + \mu(\nabla\mathbf{U}^1 + \nabla\mathbf{U}^{1T}) - (-P^2\mathbf{I} + \mu(\nabla\mathbf{U}^2 + \nabla\mathbf{U}^{2T}))$ . Traditionally one simplification is to assume that this is proportional to the mean curvature, so that  $\Delta\sigma^2 = \gamma\eta\nabla \cdot \eta$  (see [17, 50]). The second part of the surface traction is the contribution of sources of mass. Because the velocity field obtained for a single point source is known, which we can include in the final velocity since the velocity field for a point source with strength  $q$  is known, ( $\mathbf{U}_{source} = q\frac{\mathbf{x}-\mathbf{x}_0}{|\mathbf{x}-\mathbf{x}_0|}$ ), we merely add a finite number of velocity fields evaluated at the interface points (each of which is known analytically), centered at each of the points in  $\Omega^{(2)}$  to the background flow. The term  $q$  incorporates the production rate  $R$ . Therefore the velocity of each of the interface marker points is the sum of the background flow, the flow due to sources within the domain, and the solution to the integral equation

$$\begin{aligned}
 U_j(\mathbf{x}_0) = & -\frac{1}{4\pi\mu} \int_{\Gamma} \Delta\sigma^{standard}\eta_k \mathbf{G}_{ij}(\mathbf{x}, \mathbf{x}_0) dl(\mathbf{x}) \\
 & + \frac{1-\frac{1}{\lambda}}{4\pi} \int_{\Gamma} U_i(\mathbf{x}) \mathbf{T}_{ijk}(\mathbf{x}, \mathbf{x}_0)\eta_k(\mathbf{x}) dl(\mathbf{x}) \\
 & - \int_{\Omega} R\nabla\left(\frac{1}{r}\right) dV.
 \end{aligned}
 \tag{3.29}$$

We solve (3.29) using Nyström’s method [63], which requires a quadrature rule:

$$\int_a^b y(s)ds = \sum_{j=1}^n \omega_j y(s_j),$$

where  $\omega_j$  denotes the weights of the quadrature rule. Details of the implementation can be found in [17].

Once the velocity of the interface points is known, we use the method of regularized Stokeslets to obtain the velocity throughout the domain. Because the fluid velocity introduced by a finite number of isolated point forces is known analytically, one uses this representation to determine the forces that must be applied on the fluid for the velocity to match that found by the BIM equations. With the known forces, one then determines the velocity throughout the domain as a superposition of Stokeslet solutions and the background flow (including the flow due to growth within the biofilm). This method is discussed in detail elsewhere [9, 18, 20].

With the velocity in hand, we use standard techniques to solve the other equations. This includes regularizing the diffusion coefficient [18] so that the coefficients

TABLE 1  
Parameters used in the simulations.

Parameter	Symbol	Units	Value	Source
Maximum consumption rate	$\mu_s$	$\text{h}^{-1}$	0.417	[54]
Yield coefficient	$Y_b$		0.8	[54]
Monod coefficient	$K_s$	$\text{mg l}^{-1}$	0.1	[54]
$S$ influent concentration	$C_s$	$\text{mg l}^{-1}$	10	[54]
$S$ diffusion coefficient	$D_s$	$\text{m}^2\text{h}^{-1}$	$9.67 \times 10^{-6}$	[54]
$A$ diffusion coefficient	$D_a$	$\text{m}^2\text{h}^{-1}$	$1.80 \times 10^{-6}$	[54]
Diffusivity reduction	$r_*$		0.9	[56]
Length scale	$L$	$\text{m}$	$10^{-2}$	Assumed
Antimicrobial/EPS reaction rate	$\kappa$	$\text{m}^3\text{g}^{-1}\text{h}^{-1}$	10	[56]
Reaction yield	$Y_n$	$\text{g g}^{-1}$	3	[56]
Transfer rate from $B_s$ to $B_p$	$k_l$	$\text{h}^{-1}$	0.001	[14]
Transfer rate from $B_p$ to $B_s$	$k_g$	$\text{h}^{-1}$	0.05	[14]
Maximum disinfection rate	$k_d$	$\text{h}^{-1}$	40	[14]
Maximum flow rate	$U_{max}$	$\text{m h}^{-1}$	0.34	Assumed
Disinfection rate coefficient	$\alpha$		0.4	Assumed
Biofilm viscosity	$\mu^{(2)}$	$\text{cP}$	$5000 \times \text{water}$	Assumed
EPS production:				
Starvation	$k_1$	$\text{h}^{-1}$	0.79	[39]
Substrate sufficient	$k_2$	$\text{h}^{-1}$	0.18	[39]

of (3.17) and (3.18) are smooth. Another difficulty arises in the solution of (3.21), (3.20), and (3.19). Each of the state variables,  $B_s$ ,  $B_p$ , and  $E$  are zero in  $\Omega^{(1)}$ , so standard methods can lead to excessive numerical diffusion. We use a high order finite-difference approximation along with a flux limiter scheme to reduce this effect. In our application, this turns out to be less problematic than expected, since the disinfection regime actually smooths out the interface between the biofilm and the fluid.

Once the state variables are determined for a given time-step, the interface is moved according to the (calculated) interface velocity and the procedure is repeated.

**4. Simulation results.** We now describe the results of several simulations. The parameters that are used are collected in Table 1. One of the most difficult components of the system to understand is the biofilm material properties. It has been noted that the biofilm is a viscoelastic material [38, 57]. The relaxation time is quite short relative to the time scale of growth (which leads to a standard argument for using a viscous model). We use the viscosity estimated in [38], which is several orders of magnitude greater than that of the external fluid. Our results are in reasonable agreement with other models that show appreciable motion [1]. The overall goal of the simulations is to answer several specific questions regarding the outcome of periodic dosing protocols. In a series of recent papers, it was shown that the effectiveness of alternating periods of antimicrobial application with resting periods can eliminate all the bacteria, where constant dosing does not [14, 16, 42]. This mathematical observation is direct evidence of an experimental hypothesis advanced earlier [46]. However, these applications were set either in batch culture or in a chemostat setting and are not directly applicable to the problem of disinfecting bacterial biofilms. Therefore, we would like to contrast the outcomes of periodic dosing in an ODE setting with those of an extended PDE setting. Because the EPS has been shown to play a role in defending the bacteria against disinfection by reducing the antimicrobial, we will also contrast the results of simulations with and without antimicrobial/EPS reaction.

A second question concerns the mechanism of persister formation. Currently there are two hypotheses: senescence and growth-stage-mediated formation [7, 14, 16, 37, 46]. Simulation studies of senescence indicate that persisters tend to be found deep within the biofilm; at least they form above an inert region and below a layer of transition to the active surface layers.

To develop the story we will proceed with several simulations. The first set considers the behavior without disinfection and external flow. This is designed to demonstrate that, in the absence of disinfection, the domain grows appreciably. The next simply includes growth, disinfection, and fluid motion. We alternate the application time and compare the results by using a survival curve that measures the ratio of the living bacteria to the initial bacteria as a function of time. This is similar to the method used in [14, 16, 42], where the important quantity is the ratio between rest time and dose times. For simplicity here, we specify the dosing period of 12 hours and vary the rest time. We have not made any effort to keep the total applied biocide uniform across the simulations, since this is not the focus. Rather, we ask whether it is more effective to apply a constant dose or vary the dose rate. This accords with our previous results, that there is an optimal waiting time, in the sense that waiting for shorter or longer times does not clear the bacteria as quickly.

We also note that we have varied the area of the initial biofilm regions (that is, between simulations, the areas are not the same). To compare the results quantitatively, we scale each of these by the initial area (or total population). Initially, there are no persisters within the biofilm.

We then include a simple reaction and compare the survival curves for several different application times. Finally we consider the effect of the initial interface. In part this is to demonstrate that the method can address the highly heterogeneous structure and to reinforce that the geometry does play a role in the success/failure of disinfection, as seen in earlier investigations [17].

In each of these simulations we initialize the biofilm/fluid interface and apply a biocide initially for 24 hours. We then begin to alternate between periods of application and resting. During the application period, the susceptible bacteria are killed by the biocide, and persister phenotypes are exposed. During the rest period the persisters revert to susceptibles, which then reproduce. To compare our results with those of previous investigations of alternating dosing we vary the ratio of the dose and rest periods and calculate the survival curve, which is the ratio of the total bacterial population to the initial population. We also show two different aspects of the persister distribution. Because the spatial aspect depends on the dosing protocol, which is time dependent, there are differences in the spatial aspect at different times. The first comparison shows how the persister distribution develops during constant dosing for a set of initial interfaces. The second comparison shows the persister distribution after 10 days for several of the dosing regimes.

**4.1. Simulation 1: Growth, no-flow.** In this set of simulations, we assume that there is no external flow and that the nutrient is constantly fed from the sides and top of the domain. In Figure 2, we show that an isolated cluster expands due to growth in a manner similar to results from other models [19].

**4.2. Simulation 2: Growth, persister, disinfection—no reaction.** In this set of simulations we assume that the biocide does not react with components of the biofilm. Therefore these results are not applicable for a wide variety of antibiotics and biocides that are highly reactive. Here we consider four different initial interfaces: a single semicircle, two semicircles, two “mushroom”-shaped clusters, and two clusters

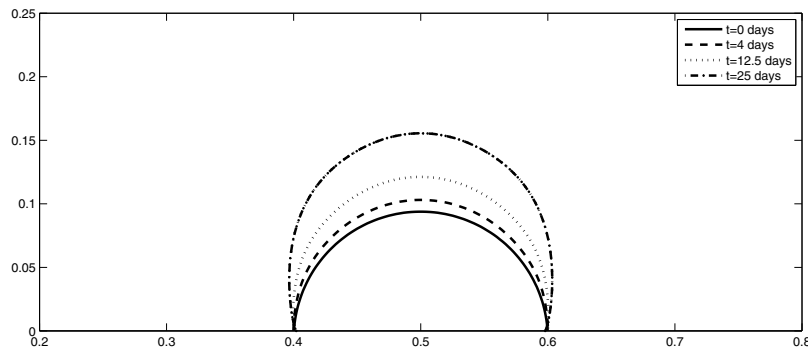


FIG. 2. *Simulating the growth of the colony in a no-flow environment. We show snapshots of the interface indicating that the colony grows in the presence of nutrient. This simulation is comparable to results using a multiphase model [19].*

that are thicker (the height of each of the interface markers is 1.5 times that of the mushroom case).

In Figure 3, we show the survival curves (starting after the initial 24 hour constant dose) for the various geometries. In general we see that the results are similar to the batch culture results—alternating dosing can be more effective as long as the rest period is not long enough to allow the population to regrow too much. We do see that the biofilm setting extends the time scale considerably, requiring dosing on the order of days rather than hours to eradicate the population. Although we have not attempted to determine the optimal ratio, it is clear that constant dosing is ineffective, as is an extended rest period.

In Figures 4–9, we show the developing distribution of persisters, susceptibles, and nutrient at different times during constant dosing for a variety of initial geometries. We note that for the two regular interfaces (semicircles), the observed persister front moves from the outside of the biofilm into the deep interior, similar to a reaction front. The persisters themselves do not migrate. Instead, the location where persisters are formed is dynamic. This is slightly different from the observations in [5], where the majority of the persisters are in the interior of the domain. In the more irregular domains, this is not always the case. In the thicker domain (Figure 9), the persisters are located both near the substratum and in the center of the cap of the mushroom. Thus, the distribution is linked to the geometry and the thickness of the biofilm. This is complicated to quantify, but it seems clear that the irregularity of typical biofilm clusters can induce irregular distribution of persister cells.

In Figures 10–13 we show the spatial distribution of persister cells after 10 days of dosing with four different rest times for each of the four initial domains. Just as the constant dosing results indicate that the geometry can induce heterogeneous distributions of persister cells, so can alternating dosing. It is interesting to note that for all nonzero rest periods it appears that there are more persisters in the upstream ends of the biofilm regions. This suggests that tolerance due to persister cells may work hand-in-hand with tolerance due to reduced nutrient availability, which protects the downstream regions [18].

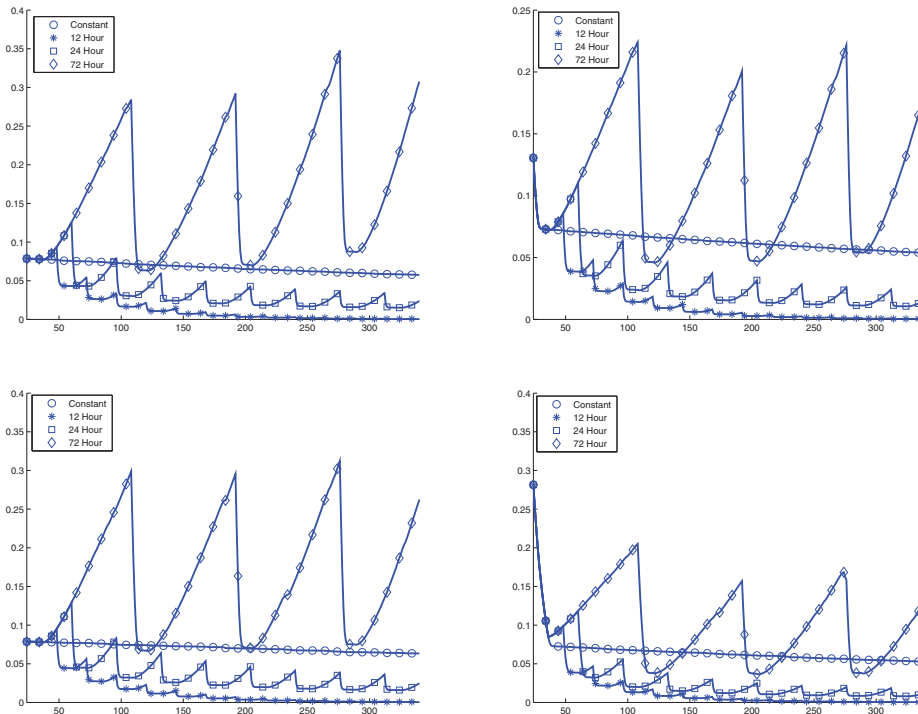


FIG. 3. Comparison of survival curves for varying rest times. Each of the four figures represents this comparison for a different initial domain geometry: single semicircle, two semicircles, short mushrooms, and tall mushrooms (clockwise from top left). There are clear quantitative differences. For example, the survival fractions for the longest rest times are larger for the domains with smaller areas (single semicircle and short mushrooms). There are no major qualitative differences—the successful regimes are the same in all simulations.

**4.3. Simulation 3: Growth and reaction.** In this simulation we allow for a reaction that destroys both the antibiotic and the EPS; see Figure 14. This reaction is assumed to be stoichiometric (e.g., the decay is proportional to the product of the densities). During rest periods, the EPS regenerates due to production by the growing bacteria. This clearly has the effect of delaying the success of the dosing strategy, since the antibiotic must first overcome the reaction to reach the bacteria. This can be seen in the time scale of the successful strategy (12 hour rest), which essentially clears the bacteria after approximately 300 hours, for the reactive case. For the nonreactive case the time to clear essentially all the bacteria was approximately two days less. Because we are also interested in the effect this has on the persister distribution, we show results only for the thick mushroom case, since the heterogeneous distribution was clearly evident in the nonreactive simulations. It is interesting to observe that the persister population seems to be enhanced downstream rather than upstream (see Figures 15 and 16). This is presumably due to the protection of the susceptible bacteria by the reactive degradation of the antibiotic. We also note that the reaction rates that we are using are based on observed penetration times for hypochlorite [56], which is less reactive than other biocides and antibiotics.

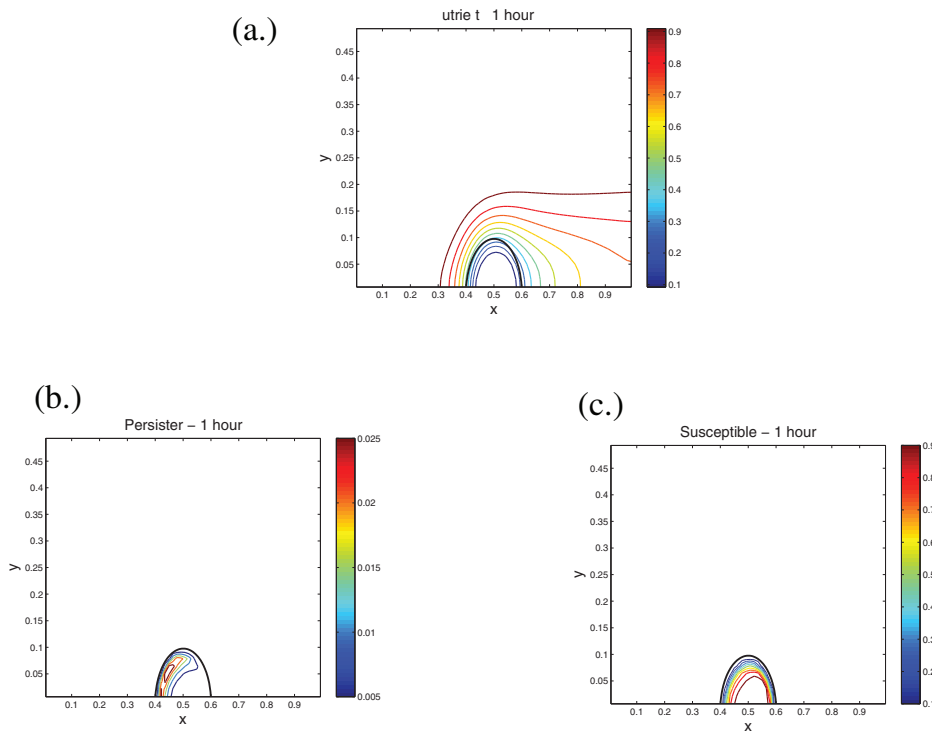


FIG. 4. We show (a) nutrient concentration, (b) persister, and (c) susceptible distribution after one hour of constant dosing. There is the development of persisters along the leading edge of the domain.

**5. Discussion.** We have extended a model of disinfection to include several important features. The focus of this investigation is the effect of persister cells on the tolerance of biofilm bacteria to antimicrobial disinfection. Because the persister hypothesis is the focus of a variety of experimental investigations, we have included a hypothetical model that is based on a previously investigated formulation. To investigate whether an alternating dosing protocol can effectively clear the bacteria, we included bacterial reproduction in our two-dimensional model. This required updating the BIM formulation that we use to pose the mathematical problem. We have also included the possibility of a reaction between the EPS and the antimicrobial.

By comparing the survival curves, we can conclude that alternating dosing can be successful in eliminating the entire population of bacteria. However, the time scale for clearance is very long in a biofilm setting compared to a batch culture or chemostat setting. This is even more of an issue if the antimicrobial is reactive. The time scale is realistic in clinical settings (e.g., typical antibiotics are used for several weeks).

We have also demonstrated that the distribution of the persister population is sensitive to the geometry, rest length, and reactivity. As in [5] there is a substantial density of persister cells deep within the biofilm; however, the distribution is not uniform. In these regions the bacteria are much less susceptible to other mechanisms of elimination. For example, the secondary immune system (e.g., phagocytes) are unable to penetrate the EPS barrier. This also means that physical removal of the biofilm colony by scraping is unlikely to be effective, since the remaining bacterial population is likely to contain persister cells. Moreover, there can be substantial

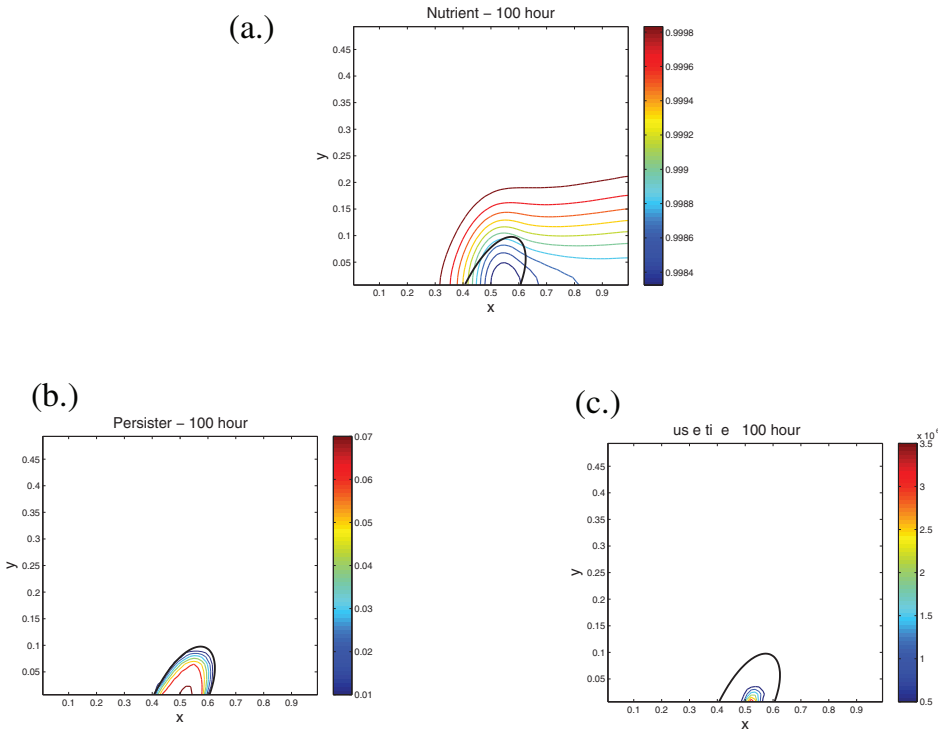


FIG. 5. We show (a) nutrient concentration, (b) persister, and (c) susceptible distribution after 100 hours of constant dosing. The persisters have extended around the exterior of the domain, while the susceptibles have been eliminated there.

concentration of persisters in the outer regions of the clusters.

It remains to quantify the window of rest lengths that is successful in clearing the bacteria. Although this could be explored computationally, the simulations are relatively time intensive—taking up to 9 hours on a small 21-node cluster of graphic processing units—limiting the parameter space that can be explored. Moreover, because the results are relatively sensitive to the geometry, it seems unlikely that a computational investigation will be practical. Even so, our analysis has indicated that many of the qualitative results obtained in a reduced setting, such as a chemostat, are preserved. The results are also robust as the parameters are changed. We did not show any results of these, since the qualitative results are quite similar.

We also note that we have assumed that the external fluid can be treated as a Stokes fluid (e.g., zero Reynolds number). This is certainly a debatable assumption, since most of the data for biofilms has been gathered in situations where the flow is not small. In fact, the Reynolds numbers in urban pipes and river applications can reach  $10^5$ , well into the turbulent regime. We first note that a derivation of the flow outside a thin biofilm leads to Stokes flow as long as the Reynolds number is “moderate” [31]. This implies that our system is likely to be reasonable for situations other than creeping flow. Moreover, the coupling of the biofilm and the external dynamics are nontrivial, and we view this as the simplest method for including disinfection and mechanical coupling. Clearly, even though the behavior is likely to be substantially different in higher Reynolds flow, our results are compatible with results from other models regarding the scale of motion [1].

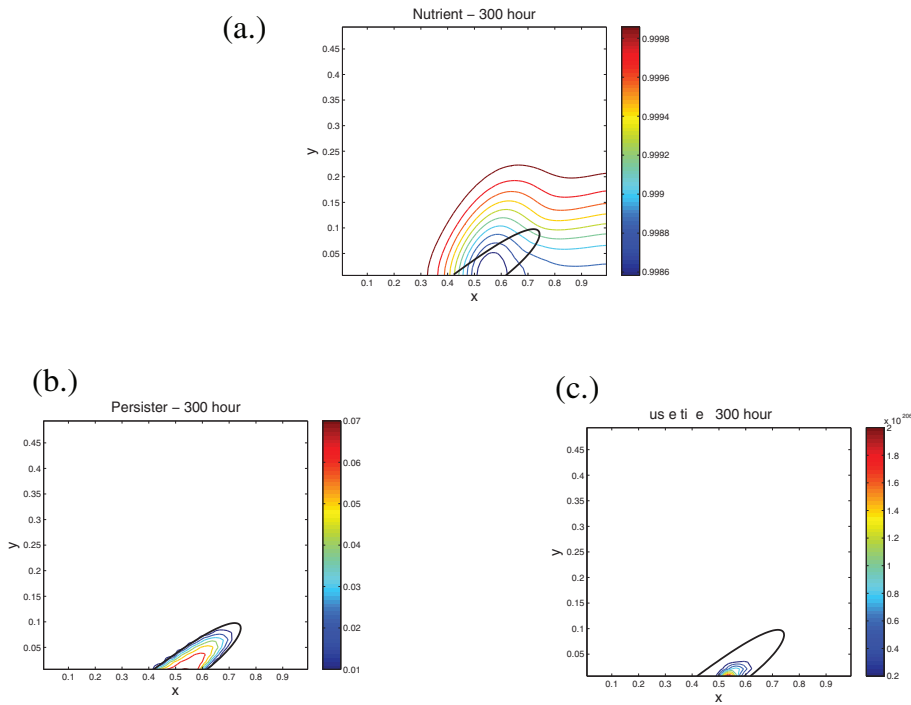


FIG. 6. We show the (a) nutrient concentration, (b) persister, and (c) susceptible distribution after 300 hours of constant dosing. The persisters are located primarily in the interior of the domain, in the same place as the susceptible population.

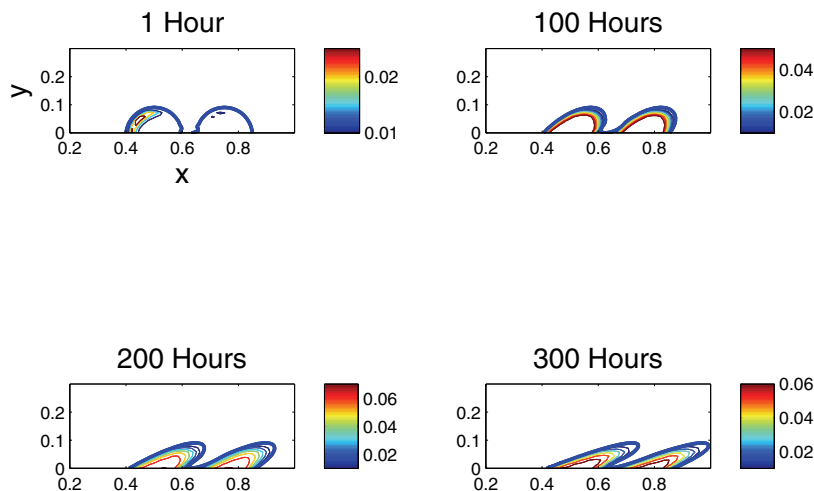


FIG. 7. The developing persister population for constant dosing is shown at different times for a biofilm that is initially two semicircles. We see that the persister population migrates from the exterior (an upstream end) of the domain into the interior of each cluster.

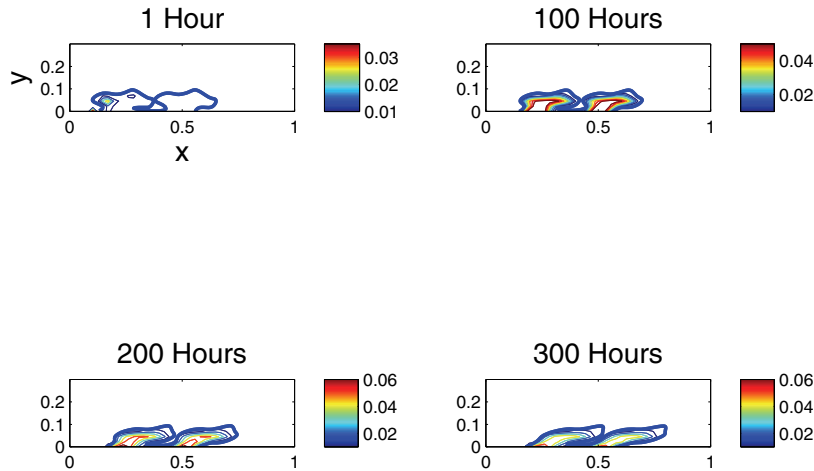


FIG. 8. The developing persister population for constant dosing is shown at different times for a biofilm that is initially two heterogeneous clusters. We see that the persister population migrates from the exterior (an upstream end) of the domain into the interior of each cluster. There is a transient island in the cap of the second mushroom seen around hour 200.

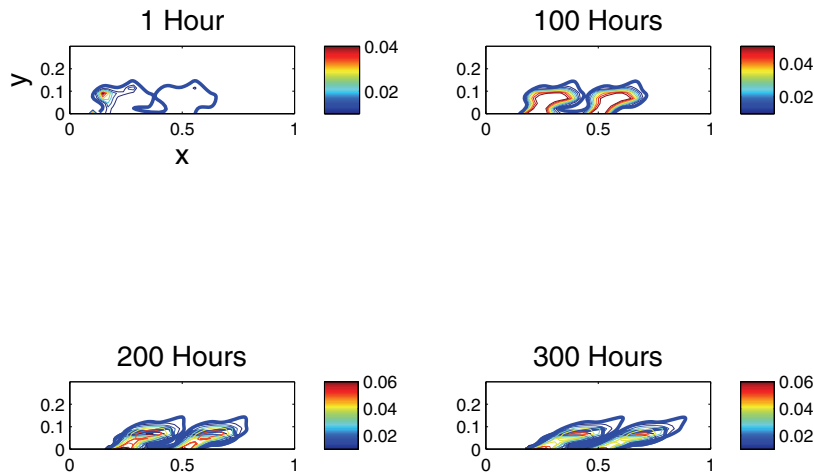


FIG. 9. The developing persister population for constant dosing is shown at different times for a biofilm that is initially two heterogeneous clusters. We see that the persister population migrates from the exterior (an upstream end) of the domain into the interior of each cluster. The transient island in the thinner cluster is now enhanced, and we have two regions of high persister cells in each cluster.

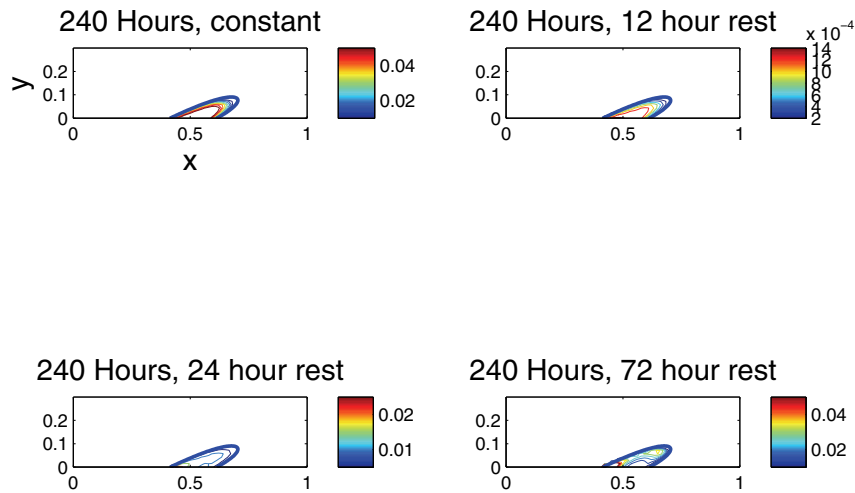


FIG. 10. *The persister distribution after 10 days for the biofilm that is initially a single semicircle. We show constant, 12 hour rest, 24 hour rest, and 72 hour rest. It is just possible to see that for the longer rest periods there are more persisters in the upstream end of the domain.*

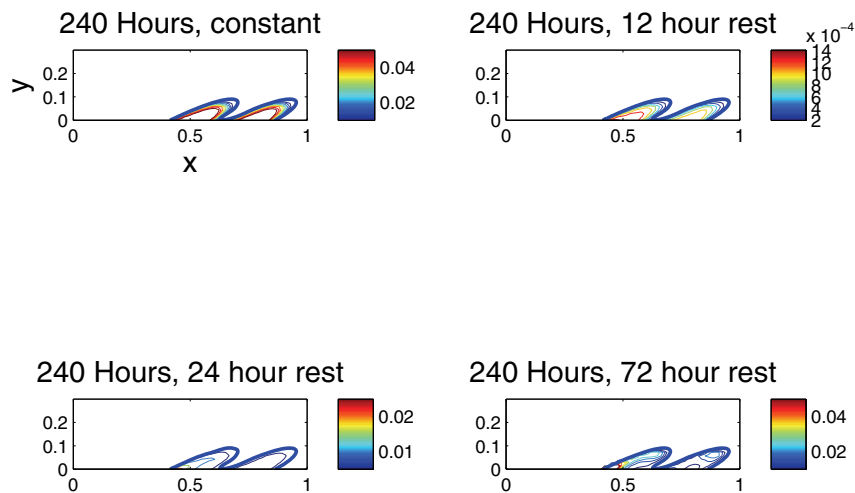


FIG. 11. *The persister distribution after 10 days for the biofilm that is initially two semicircles. We show constant, 12 hour rest, 24 hour rest, and 72 hour rest. We see that for the longer rest periods there are more persisters in the upstream end of the domain and an island at the top of the downstream portion.*

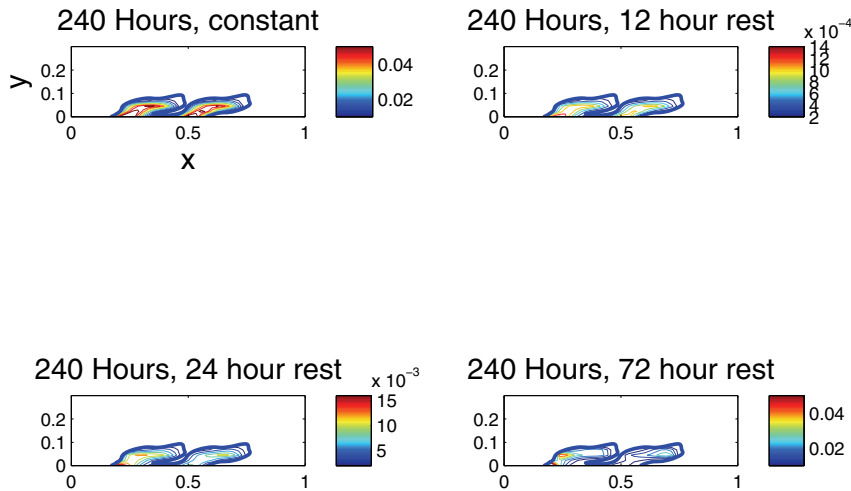


FIG. 12. The persister distribution after 10 days for the biofilm that is initially two mushrooms. We show constant, 12 hour rest, 24 hour rest, and 72 hour rest. We see that for the longer rest periods there are more persisters in the upstream end of the domain and an island at the top of the downstream portion.

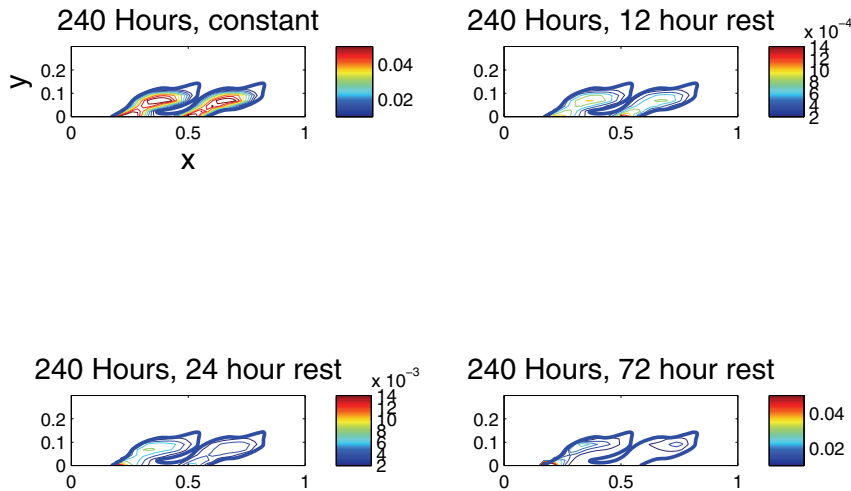


FIG. 13. The persister distribution after 10 days for the biofilm that is initially two thicker mushrooms. We show constant, 12 hour rest, 24 hour rest, and 72 hour rest. We see that for the longer rest periods there are more persisters in the upstream end of the domain and an island at the top of the downstream portion.

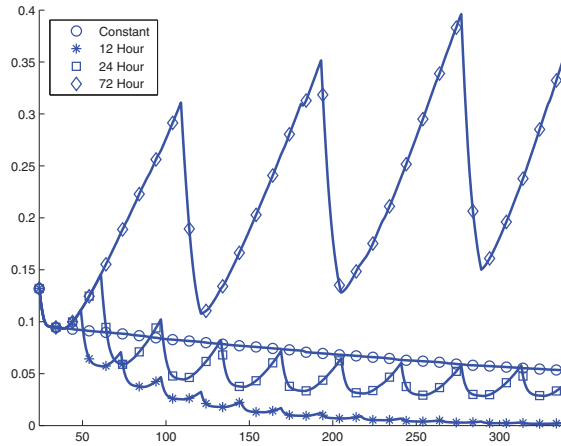


FIG. 14. Survival curves for the thicker mushroom domain and including a stoichiometric reaction between the EPS and the antibiotic. We see that the reaction does not alter the qualitative results but does delay the clearance of the bacteria.

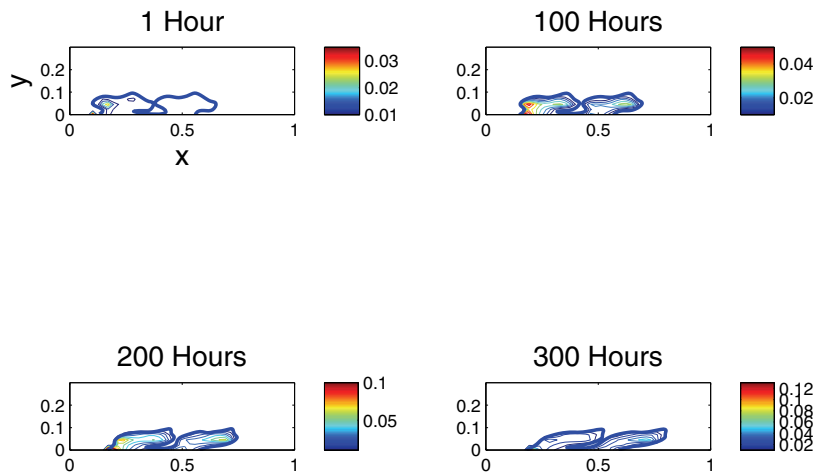


FIG. 15. The developing persister population for constant dosing with a reactive antibiotic is shown at different times for a biofilm that is initially two heterogeneous clusters. We see that the persister population migrates from the exterior (an upstream end) of the domain into the interior of each cluster. The persister population seems to be less sharply contained at the end of the simulation, indicating that the persisters are more evenly distributed if there is a degrading reaction.

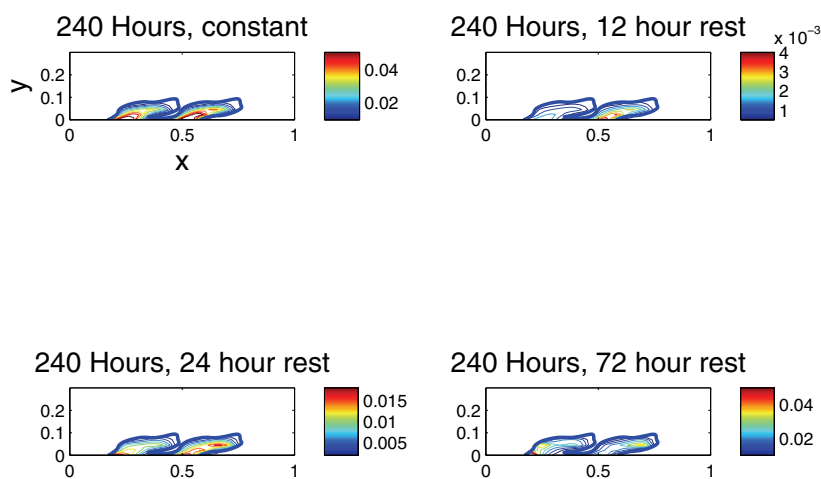


FIG. 16. The persister distribution after 10 days for the biofilm that is initially two thicker mushrooms. We show constant, 12 hour rest, 24 hour rest, and 72 hour rest. We see that for the longer rest periods there are more persisters in the upstream end of the domain and an island at the top of the downstream portion, although this is much less sharply defined than in the nonreactive case.

## REFERENCES

- [1] E. ALPKVIST AND I. KLAPPER, *Description of mechanical response including detachment using a novel particle method of biofilm/flow interaction*, Water Sci. Tech., 55 (2007), pp. 265–273.
- [2] J. N. ANDERL, M. J. FRANKLIN, AND P. S. STEWART, *Role of antibiotic penetration limitation in Klebsiella pneumoniae biofilm resistance to ampicillin and ciprofloxacin*, Antimicrobial Agents and Chemotherapy, 44 (2000), pp. 1818–1824.
- [3] K. ANGUIGE, J. KING, AND J. WARD, *Modelling antibiotic- and anti-quorum sensing treatment of a spatially-structured Pseudomonas aeruginosa population*, J. Math. Biol., 51 (2005), pp. 557–594.
- [4] K. ANGUIGE, J. KING, J. WARD, AND P. WILLIAMS, *Mathematical modelling of therapies targeted at bacterial quorum sensing*, Math. Biosci., 192 (2004), pp. 39–83.
- [5] B. P. AYATI AND I. KLAPPER, *A multiscale model of biofilm as a senescence-structured fluid*, Multiscale Model. Simul., 6 (2007), pp. 347–365.
- [6] R. BAKKE, M. G. TRULEAR, J. A. ROBINSON, AND W. G. CHARACKLIS, *Activity of Pseudomonas aeruginosa in biofilms: Steady state*, Biotechnol. Bioeng., 26 (2004), pp. 1418–1424.
- [7] N. Q. BALABAN, J. MERRIN, R. CHAIT, L. KOWALIK, AND S. LEIBLER, *Bacterial persistence as a phenotypic switch*, Science, 305 (2005), pp. 1622–1625.
- [8] G. BATCHELOR, *An Introduction to Fluid Dynamics*, Cambridge University Press, Cambridge, UK, 1967.
- [9] J. T. BEALE AND M.-C. LAI, *A method for computing nearly singular integrals*, SIAM J. Numer. Anal., 38 (2001), pp. 1902–1925.
- [10] J. D. CHAMBLESS, S. M. HUNT, AND P. S. STEWART, *A three-dimensional computer model of four hypothetical mechanisms protecting biofilms from antimicrobials*, Appl. Environ. Microbiol., 72 (2006), pp. 2005–2013.
- [11] W. CHARACKLIS, *Biofilms*, John Wiley & Sons, New York, 1990.
- [12] X. CHEN AND P. STEWART, *Role of electrostatic interactions in cohesion of bacterial biofilms*, Appl. Microbiol. Biotechnol., 59 (2002), pp. 718–720.
- [13] N. G. COGAN, *The role of the biofilm matrix in structural development*, Math. Medicine Biol., 21 (2004), pp. 147–166.
- [14] N. G. COGAN, *Effects of persister formation on bacterial response to dosing*, J. Theoret. Biol., 238 (2006), pp. 694–703.
- [15] N. G. COGAN, *Hybrid numerical treatment of two fluid problems with passive interfaces*, Comm. Appl. Math. Comput. Sci., 2 (2007), pp. 117–133.

- [16] N. G. COGAN, *Incorporating toxin hypothesis into a mathematical model of persister formation and dynamics*, J. Theoret. Biol., 248 (2007), pp. 340–349.
- [17] N. G. COGAN, *A two-fluid model of biofilm disinfection*, Bull. Math. Biol., 70 (2008), pp. 800–819.
- [18] N. G. COGAN, R. CORTEZ, AND L. J. FAUCI, *Modeling physiological resistance in bacterial biofilms*, Bull. Math. Biol., 67 (2005), pp. 831–853.
- [19] N. G. COGAN AND J. P. KEENER, *The role of the biofilm matrix in structural development*, Math. Med. Biol., 21 (2004), pp. 147–166.
- [20] R. CORTEZ, *The method of regularized Stokeslets*, SIAM J. Sci. Comput., 23 (2001), pp. 1204–1225.
- [21] R. CORTEZ, L. FAUCI, AND A. MEDOVNIKOV, *The method of regularized Stokeslets in three dimensions: Analysis, validation, and application to helical swimming*, Phys. Fluids., 17 (2005), pp. 1–14.
- [22] J. COSTERTON, *Cystic fibrosis pathogenesis and the role of biofilms in persistent infection*, Trends Microbiol., 9 (2001), pp. 50–52.
- [23] J. COSTERTON, P. STEWART, AND E. GREENBERG, *Bacterial biofilms: A common cause of persistent infections*, Science, 284 (1999), pp. 1318–1322.
- [24] J. W. COSTERTON, K. J. CHENG, G. G. GEESEY, T. I. LADD, J. C. NICKEL, M. DASGUPTA, AND T. J. MARRIE, *Bacterial biofilms in nature and disease*, Annu. Rev. Microbiol., 41 (1987), pp. 435–464.
- [25] V. CRISTINI, J. BLAWZDZIEWICZ, AND M. LOEWENBERG, *Drop breakup in three-dimensional viscous flows*, Phys. Fluids Lett., 10 (1998), pp. 1781–1783.
- [26] F. R. CUNHA, A. J. DE SOUSAI, AND M. LOEWENBERG, *A mathematical formulation of the boundary integral equations for a compressible Stokes flow*, Math. Appl. Comput., 22 (2003), pp. 53–73.
- [27] D. DAVIES, *Understanding biofilm resistance to antibacterial agents*, Nature Rev. Drug Discovery, 2 (2003), pp. 114–122.
- [28] M. DESAI, T. BUHLER, P. WELLER, AND M. BROWN, *Increasing resistance of planktonic and biofilm cultures of Burkholderia cepacia to ciprofloxacin and ceftazidime during exponential growth*, J. Antimicrobial Chemotherapy, 42 (1998), pp. 153–160.
- [29] J. DOCKERY AND I. KLAPPER, *Finger formation in biofilm layers*, SIAM J. Appl. Math., 62 (2001), pp. 853–869.
- [30] M. G. DODDS, K. J. GROBE, AND P. S. STEWART, *Modeling biofilm antimicrobial resistance*, Biotechnol. Bioeng., 68 (2000), pp. 456–465.
- [31] H. J. EBERL AND R. SUDARSAN, *Exposure of biofilms to slow flow fields: The convective contribution to growth and disinfection*, J. Theoret. Biol., 253 (2008), pp. 788–807.
- [32] P. GILBERT AND M. R. W. BROWN, *Mechanisms of the protection of bacterial biofilms from antimicrobial agents*, in Microbial Biofilms, H. M. Lappin-Scott and J. W. Costerton, eds., Cambridge University Press, Cambridge, UK, 1995, pp. 118–130.
- [33] T. Y. HOU, J. S. LOWENGRUB, AND M. J. SHELLEY, *Boundary integral methods for multicomponent fluids and multiphase fluids*, J. Comput. Phys., 169 (2001), pp. 302–362.
- [34] M. IMRAN AND H. L. SMITH, *The pharmacodynamics of antibiotic treatment*, J. Comput. Math. Methods Med., 7 (2006), pp. 229–263.
- [35] I. KEREN, N. KALDALU, A. SPOERING, Y. WANG, AND K. LEWIS, *Persister cells and tolerance to antimicrobials*, FEMS Microbiol. Lett., 230 (2004), pp. 13–18.
- [36] I. KEREN, D. SHAH, A. SPOERING, N. KALDALU, AND K. LEWIS, *Specialized persister cells and the mechanism of multidrug tolerance in Escherichia coli*, J. Bacteriol., 186 (2004), pp. 8172–8180.
- [37] I. KLAPPER, P. GILBERT, B. P. AYATI, J. DOCKERY, AND P. S. STEWART, *Senescence can explain microbial persistence*, Microbiology, 153 (2007), pp. 3623–3630.
- [38] I. KLAPPER, C. RUPP, R. CARGO, B. PURVEDORJ, AND P. STOODLEY, *Viscoelastic fluid description of bacterial biofilm material properties*, Biotechnol. Bioeng., 80 (2002), pp. 289–296.
- [39] J. D. R. KOMMEDAL, R. BAKKE, AND P. STOODLEY, *Modelling production of extracellular polymeric substances in a Pseudomonas aeruginosa chemostat culture*, Water Sci. Technol., 43 (2001), pp. 129–134.
- [40] J.-U. KREFT, C. PICIOREANU, J. W. T. WIMPENNY, AND M. C. M. VAN LOOSDRECHT, *Individual-based modelling of biofilms*, Environ. Microbiol., 147 (2001), pp. 2897–2912.
- [41] A. T. LAYTON, *An efficient numerical method for the two-fluid Stokes equations with a moving boundary*, Comput. Methods Appl. Mech. Engrg., 197 (2007), pp. 2147–2155.
- [42] P. DE LEENHEER AND N. G. COGAN, *Failure of antibiotic treatment in microbial populations*, J. Math. Biol., 59 (2009), pp. 563–579.
- [43] A. P. LENZ, K. S. WILLIAMSON, B. PITTS, P. S. STEWART, AND M. J. FRANKLIN, *Localized*

- gene expression in Pseudomonas aeruginosa biofilms*, Appl. Environ. Microbiol., 74 (2008), pp. 4463–4471.
- [44] R. J. LEVEQUE AND Z. LI, *The immersed interface method for elliptic equations with discontinuous coefficients and singular sources*, SIAM J. Numer. Anal., 31 (1994), pp. 1019–1044.
- [45] B. R. LEVIN AND D. E. ROZEN, *Noninherited antibiotic resistance*, Nature Rev. Microbiol., 4 (2006), pp. 556–562.
- [46] K. LEWIS, *Riddle of biofilm resistance*, Antimicrobial Agents and Chemotherapy, 45 (2001), pp. 999–1007.
- [47] S. MOLLER, C. STERNBERG, J. B. ANDERSEN, B. B. CHRISTENSEN, J. L. RAMOS, M. GIVSKOV, AND S. MOLIN, *In situ gene expression in mixed-culture biofilms: Evidence of metabolic interactions between community members*, Appl. Environ. Microbiol., 64 (1998), pp. 721–732.
- [48] C. PICIOREANU, M. C. M. VAN LOOSDRECHT, AND J. J. HEIJNEN, *Mathematical modeling of biofilm structure with a hybrid differential-discrete cellular automaton approach*, Biotechnol. Bioeng., 58 (2000), pp. 101–116.
- [49] L. K. POULSEN, G. BALLARD, AND D. A. STAHL, *Use of rRNA fluorescence in situ hybridization for measuring the activity of single cells in young and established biofilms*, Appl. Environ. Microbiol., 59 (1993), pp. 1354–1360.
- [50] C. POZRIKIDIS, *Boundary Integral and Singularity Methods for Linearized Viscous Flow*, Cambridge University Press, Cambridge, UK, 1992.
- [51] C. POZRIKIDIS, *Expansion of a compressible gas bubble in Stokes flow*, J. Fluid Mech., 442 (2001), pp. 171–189.
- [52] C. POZRIKIDIS, *Interfacial dynamics for Stokes flow*, J. Comput. Phys., 169 (2001), pp. 250–301.
- [53] C. POZRIKIDIS, *Modeling and Simulation of Capsules and Biological Cells*, Chapman & Hall/CRC Press, London/Boca Raton, FL, 2003.
- [54] M. E. ROBERTS AND P. S. STEWART, *Modeling antibiotic tolerance in biofilms by accounting for nutrient limitation*, Antimicrobial Agents and Chemotherapy, 48 (2004), pp. 48–52.
- [55] J. A. ROBINSON, M. G. TRULEAR, AND W. G. CHARACKLIS, *Cellular reproduction and extracellular polymer formation by Pseudomonas aeruginosa in continuous culture*, Biotechnol. Bioeng., 26 (1984), pp. 1409–1417.
- [56] S. S. SANDERSON AND P. S. STEWART, *Evidence of bacterial adaptation to monochloramine in Pseudomonas aeruginosa biofilms and evaluation of biocide action model*, Biotechnol. Bioeng., 56 (1997), pp. 201–209.
- [57] T. SHAW, M. WINSTON, C. J. RUPP, I. KLAPPER, AND P. STOODLEY, *Commonality of elastic relaxation times in biofilms*, Phys. Rev. Lett., 93 (2004), paper 098102.
- [58] P. STEWART, J. RAYNER, F. ROE, AND W. REES, *Biofilm penetration and disinfection efficacy of alkaline hypochlorite and chlorosulfamates*, J. Appl. Microbiol., 91 (2001), pp. 525–532.
- [59] P. S. STEWART, *Theoretical aspects of antibiotic diffusion into microbial biofilms*, Antimicrobial Agents and Chemotherapy, 40 (1996), pp. 2517–2522.
- [60] P. STOODLEY, R. CARGO, C. J. RUPP, S. WILSON, AND I. KLAPPER, *Biofilm material properties as related to shear-induced deformation and detachment phenomena*, J. Industrial Microbiol. Biotech., 361 (2002), pp. 1476–5535.
- [61] N. SUFYA, D. ALLISON, AND P. GILBERT, *Clonal variation in maximum specific growth rate and susceptibility towards antimicrobials*, J. Appl. Microbiol., 95 (2003), pp. 1261–1267.
- [62] B. SZOMOLAY, I. KLAPPER, J. DOCKERY, AND P. S. STEWART, *Adaptive responses to antimicrobial agents in biofilms*, Environ. Microbiol., 7 (2005), pp. 1186–1191.
- [63] W. T. VETTERLING, S. A. TEUKOLSKY, W. H. PRESS, AND B. FLANNERLY, *Numerical Recipes in C: The Art of Scientific Computing*, Cambridge University Press, Cambridge, UK, 2002.
- [64] O. WANNER AND W. GUJER, *A multispecies biofilm model*, Biotechnol. Bioeng., 28 (1986), pp. 314–328.
- [65] O. WANNER AND E. MORGENROTH, *Biofilm modeling with AQUASIM*, Water Sci. Technol., 49 (2004), pp. 137–144.
- [66] P. WATNICK AND R. KOLTER, *Biofilm, City of microbes*, J. Bacteriol., 182 (2000), pp. 2675–2679.
- [67] J. W. WIMPENNY AND R. COLASANTI, *A unifying hypothesis for the structure of microbial biofilms based on cellular automaton models*, FEMS Microbiol. Ecol., 22 (2006), pp. 1–16.
- [68] K. D. XU, G. A. MCFETERS, AND P. S. STEWART, *Biofilm resistance to antimicrobial agents*, Microbiology, 146 (2000), pp. 547–549.
- [69] T. ZHANG, N. G. COGAN, AND Q. WANG, *Field-phase models for biofilms. II. 2-d numerical simulations of biofilm-flow interaction*, Comm. Comput. Phys., 4 (2008), pp. 72–101.
- [70] T. ZHANG, N. G. COGAN, AND Q. WANG, *Phase field models for biofilms. I. Theory and one-dimensional simulations*, SIAM J. Appl. Math., 69 (2008), pp. 641–669.